ORIGINAL ARTICLE

JBMR®

Limitations of Global Morphometry in Predicting Trabecular Bone Failure

Martin Stauber,[1,2] Ara Nazarian,[3] and Ralph Müller[1]

[1]Institute for Biomechanics, Eidgenössische Technische Hochschule (ETH) Zurich, Zurich, Switzerland
[2]b-cube AG, Brüttisellen, Switzerland
[3]Center for Advanced Orthopaedic Studies, Beth Israel Deaconess Medical Center and Harvard Medical School, Boston, MA, USA

ABSTRACT

Efforts in finding independent measures for accurate and reliable prediction of trabecular bone failure have led to the development of a number of morphometric indices characterizing trabecular bone microstructure. Generally, these indices assume a high homogeneity within the bone specimen. However, in the present study we found that the variance in bone volume fraction (BV/TV) in a single bone specimen can be relatively large (CV = 9.07% to 28.23%). To assess the limitations of morphometric indices in the prediction of bone failure for specimens in which the assumption of homogeneity is not met, we harvested 13 cadaveric samples from a single human spine. We tested these cylindrical samples using image-guided failure assessment (IGFA), a technique combining stepwise microcompression and time-lapsed micro–computed tomography (μCT). Additionally, we computed morphometric indices for the entire sample as well as for 10 equal subregions along the anatomical axis. We found that ultimate strength was equally well predicted by BV/TV of the entire sample ($R^2 = 0.55$) and BV/TV of the weakest subregion ($R^2 = 0.57$). Investigating three-dimensional animations of structural bone failure, we showed that two main failure mechanisms determine the competence of trabecular bone samples; in homogeneous, isotropic trabecular bone samples, competence is determined by a whole set of trabecular elements, whereas in inhomogeneous, anisotropic bone samples a single or a missing trabeculae may induce catastrophic failure. The latter failure mechanism cannot be described by conventional morphometry, indicating the need for novel morphometric indices also applicable to the prediction of failure in inhomogeneous bone samples. © 2014 American Society for Bone and Mineral Research.

KEY WORDS: MORPHOMETRY; COMPRESSION TESTING; IGFA; AVERAGE PROPERTIES; LIMITATIONS

Introduction

Osteoporosis is now recognized as one of the major public health problems facing postmenopausal women and aging individuals irrespective of gender.[1] It is defined as a skeletal disorder characterized by compromised bone strength predisposed to an increased risk of fracture. Bone strength reflects the integration of two main features: bone mineral density expressed as grams of mineral per area/volume and bone quality, referring to bone architecture, turnover, damage accumulation, collagen cross-linking, and bone mineralization.[2]

To assess bone strength, different experimental testing methods have been proposed.[3] For trabecular bone biopsies and autopsies, compression[4–11] and tensile testing[6,7] have been used to assess apparent Young's modulus and ultimate strength. Compression testing has been expanded to a method called image-guided failure assessment (IGFA),[12] which incorporates stepwise microcompression in combination with time-lapse micro–computed tomography (μCT). This method allows for the assessment of mechanical data in addition to providing three-dimensional (3D) images that enable one to visually study the 3D failure behavior of cellular solids.[13–15]

The assessment and prediction of bone strength has traditionally been related to independent measures aimed at explaining the variation in stiffness and strength. An index of note is the bone volume fraction (BV/TV), which has been shown to explain a large portion of the variation in both stiffness and strength.[16–18] However, it has also been recognized that older persons may lose bone, as expressed by a decrease in bone density, but do not develop fractures because bone mineral density, bone geometry, bone microarchitecture, and bone material properties are all contributing components which determine bone strength.[19,20] For this reason, efforts in the quantification of structural properties have gained in prominence, and many different methods have been proposed to further describe the influence of changes in bone microstructure onto its mechanical properties.[21–29] However, these methods typically present average numbers for the entire specimen, therefore inhomogeneities and local variations in these indices are ignored. It is possible that these inhomogeneities may locally

Received in original form January 21, 2013; revised form May 10, 2013; accepted June 3, 2013. Accepted manuscript online June 12, 2013.
Address correspondence to: Martin Stauber, PhD, b-cube AG, Fabrikweg 2, CH-8306 Brüttisellen, Switzerland. E-mail: mstauber@b-cube.ch
Additional Supporting Information may be found in the online version of this article.

Journal of Bone and Mineral Research, Vol. 29, No. 1, January 2014, pp 134–141
DOI: 10.1002/jbmr.2006
© 2014 American Society for Bone and Mineral Research

weaken the trabecular bone structure and finally initiate failure. This calls into question the reliability of failure prediction based on average morphometric indices and the appropriate interpretation of mechanical results from compression testing. It is further unclear whether the microstructural and mechanical properties of a biopsy or autopsy are representative measures for the microstructural and mechanical properties of its parent organ.

In this study, we used results from IGFA experiments in combination with morphometric indices to analyze the relative effect of local bone structure variations on the mechanical properties of trabecular bone samples. Bone samples were harvested from a single donor to analyze intraperson variability of trabecular bone and to estimate how well the properties of autopsies reflect the properties of the parent organ. Additionally, we aimed to visually identify differences in failure modes for different structure types. We believe that these observations highlight the limitations of the strength prediction of whole bones based on uniaxial compression testing experiments or average morphometry of biopsy and autopsy samples, such as iliac crest specimens used for structure assessment in clinical studies or bone cores used for mechanical testing in basic bone research.

We hypothesized that the prediction of bone failure by global morphometric indices is limited because of the inhomogeneity of trabecular bone. We suggest that homogeneous bone specimens fail in well-defined bands, whereas inhomogeneous bone specimens fail in a catastrophic mode that causes the whole bone to collapse at once. Furthermore, we hypothesized that the morphometric and mechanical properties of autopsies and biopsies may not be reflecting the morphometric and mechanical properties of the whole organ.

Materials and Methods

A group of 13 human vertebral trabecular bone specimens were cored ($Ø = 7.85 \pm 0.21$ mm) from thoracic and lumbar vertebral bodies of one donor (65-year-old male) from the Anatomic Gift Program at Harvard University. The bone specimens were cored parallel to the anatomical axis out of a precut block of vertebral trabecular bone using a diamond coring-tool (Starlite Industries; Rosemont, PA, USA) while completely submerged in 0.9% saline solution. All specimens were stored in saline-soaked gauze at a temperature of –20°C. Once cored, both ends of all specimens were cut perpendicular to the cylindrical axis between two parallel diamond blades running on a low-speed saw (Isomet; Buehler Corp., Lake Bluff, IL, USA) operating under copious irrigation (height [H] $= 11.62 \pm 0.14$ mm).

Prior to testing, prealigned brass end caps ($Ø = 9$ mm, $H = 1.2$ mm) were glued to both ends of the specimens. This step reduced end artifact by restraining displacement at either end of the specimen and by providing support to free trabecular elements.[30] The specimens remained wet during testing with the humidity sealed within the microcompression device; this was verified upon retrieval of wet specimens at the end of the testing period.

Data was acquired with IGFA using a previously described mechanical testing and data acquisition (MTDAQ) device.[13,14,31] All specimens were preconditioned to eliminate typical toe behavior[5,32] at a strain rate of 0.005%/s for seven cycles. The specimens underwent sequential compressive steps of 0%, 4%, 8%, 12%, 16%, and 20% nominal strain.

Progressive images were generated using a microtomographic imaging system (μCT 20; Scanco Medical AG, Brüttisellen, Switzerland).[33–40] These measurements were stored in 3D image arrays with isotropic voxel sizes of 34 μm. A 3D Gaussian filter with a limited, finite filter width ($\sigma = 1.2$) and support[1] was used to partially suppress noise in the volumes. These images were binarized to separate bone from background using a global thresholding procedure with threshold value of 22.4%.[41] A component labeling algorithm (IPL; Scanco Medical AG, Brüttisellen, Switzerland) was applied to keep only the largest connected bone-component and to remove small particles arising from noise and artifacts.

Each specimen's μCT image was divided along the cylinder axis into 10 subregions of equal height (Fig. 1). Conventional morphometric indices were computed for each of these subregions as well as for the entire specimen. The morphometric indices were obtained according to Hildebrand and colleagues[42]: bone volume fraction (BV/TV), specific bone surface density (BS/BV), trabecular bone pattern factor (TBPf), trabecular number (Tb.N), trabecular thickness (Tb.Th), trabecular separation (Tb.Sp), degree of anisotropy (DA), and connectivity density (Conn.D).

The 3D images of each compression step were combined into an animation, because 3D animations of the mechanical experiments contribute significantly to the understanding of specimen failure. For this purpose, the 3D images had to be aligned initially with respect to the bottom endplate, because this plate was fixed during the experiment. An algorithm was used to find the last plane of this endplate in each 3D image, enabling an alignment of the images along the perpendicular axis. A subsequent two-dimensional (2D) correlation procedure was used in the first five bottom planes in order to perform alignment. Each aligned 3D dataset was then visualized under the same conditions (orientation, light settings) by using an extended marching cubes algorithm.[43] The resulting images were finally turned into an animation to visualize failure for all specimens; a selection is shown in Figs. 2 and 3. All animations are provided as online Supporting Information. This procedure was repeated in four main directions (front, left, back, right) for

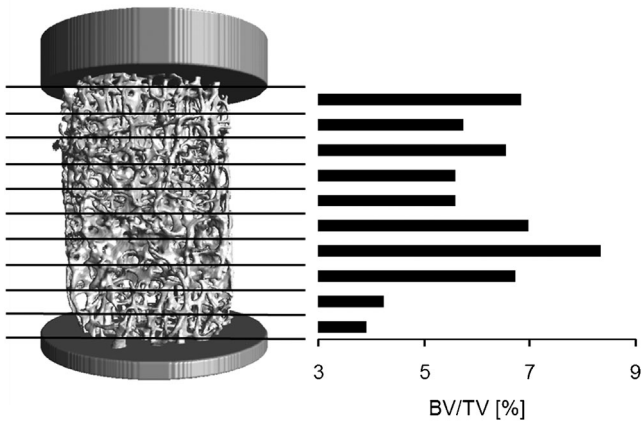

Fig. 1. Regional morphometry: the sample was subdivided into 10 subregions along the anatomical axis. BV/TV was computed for each subregion. BV/TV = bone volume fraction.

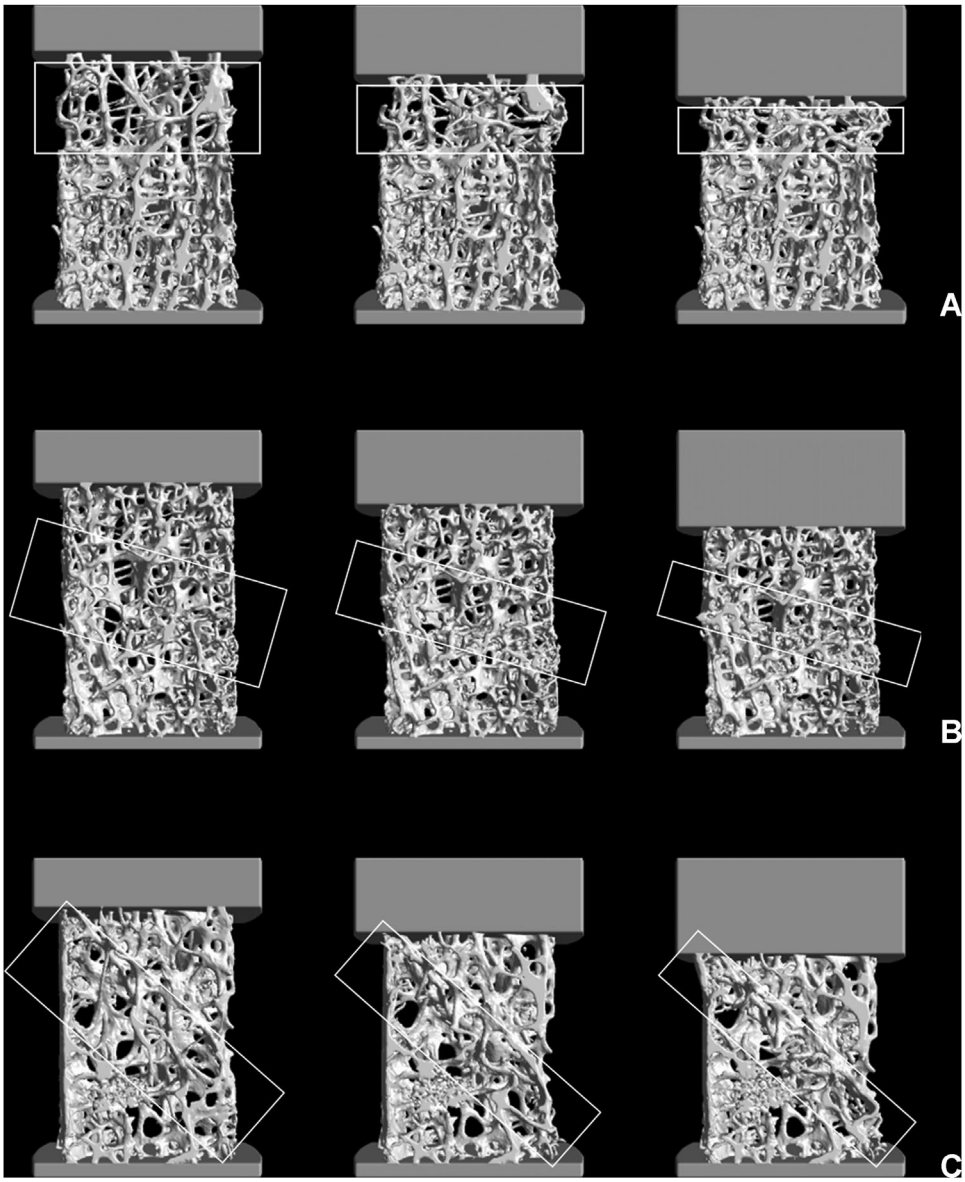

Fig. 2. Band-like local failure in (*A*) compression, (*B*) compression/shear, and (*C*) shear failure mode. These samples failed in a relatively well defined band (box) whereas the other regions hardly underwent any visible postyield deformation. Each row shows a specimen in three successive compression steps (0%, 8%, 16% apparent strain).

the whole specimen as well as in two directions (front, left) for 110 central axial slices (3.74 mm).

Results

All samples presented were harvested from one donor. The variation within the morphometric indices was large for this donor (Table 1). Also, Figs. 2 and 3 revealed a variety of visual configurations for bone microstructure.

In Fig. 2, the 110 axial mid-slices of three relatively homogeneous isotropic samples are shown in three successive compression steps (0%, 8%, 16% apparent strain). All three samples failed in well-defined bands; the failure band in the sample in Fig. 2*A* is almost horizontal and completely diagonal in the sample in Fig. 2*C*. Thus, in the sample Fig. 2*A* compression is the predominant mode of failure, whereas in the sample in Fig. 2*C* shear failure is the predominant mode. In the sample in Fig. 2*B* the failure band had a relatively small angle to the cylinder axis, and it can be expected that in this sample shear and compression forces determine failure. It is noteworthy that in both samples the regions outside the box hardly underwent any visible deformation, because no failure is obvious.

In Fig. 3, the 110 axial mid-slices of three inhomogeneous and anisotropic samples are shown in three successive compression steps (0%, 8%, 16% apparent strain). In contrast to the samples in Fig. 2, these structures did not fail in a well-defined band but instead failed catastrophically over the entire length of the sample. The arrow in Fig. 3*A* points to a relatively large plate-like element undergoing complete bending during compression.

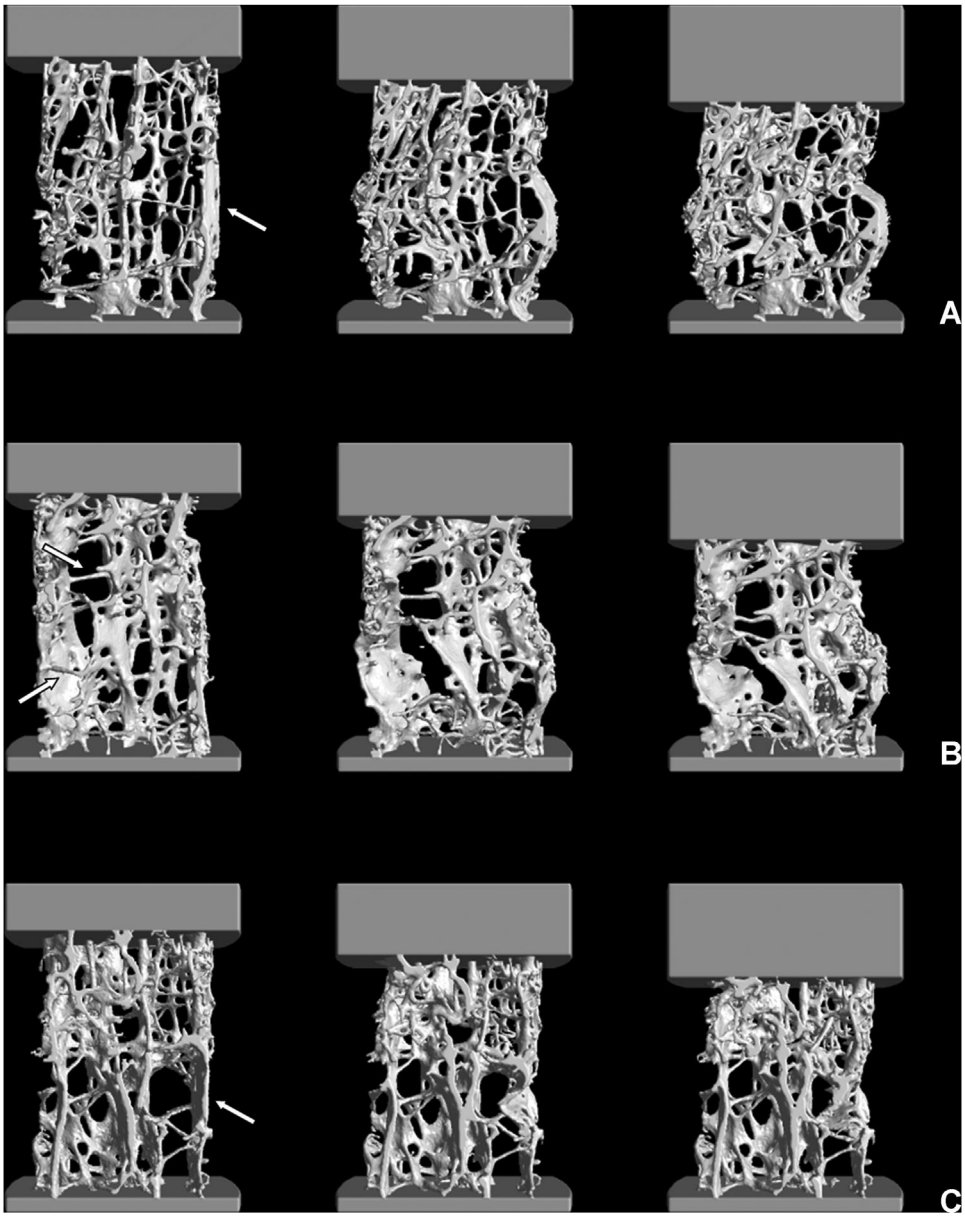

Fig. 3. Catastrophic failure modes: all samples failed over the entire length due to missing interconnecting trabeculae. (*A*) Missing interconnecting horizontal trabecular elements cause the large plate-like element (arrow) to undergo complete bending during compression. (*B*) The two interconnecting horizontal trabeculae (arrows) fail in bending (upper) and tension (lower) during compression. (*C*) The vertical plate-like element (arrow) fails due to missing interconnecting trabeculae. Each row shows a specimen in three successive compression steps (0%, 8%, 16% apparent strain).

Table 1. Variations Within the Morphometric Indices for This Donor

	BV/TV (%)	BS/BV (mm^2/mm^3)	SMI (1)	TBPf (1/mm)	DA (1)	Tb.Th (mm)	Tb.Sp (mm)	Conn.D (1/mm)
Minimum	4.19	15.44	1.62	4.30	1.21	0.146	1.011	0.58
Maximum	12.33	20.79	2.18	7.12	1.53	0.204	1.589	2.15
Mean	7.82	17.95	1.92	5.77	1.40	0.170	1.266	1.37
SD	2.02	1.51	0.16	0.82	0.11	0.015	0.212	0.54
CV	25.8	8.4	8.3	14.3	7.8	8.7	16.7	39.8

BV/TV = bone volume fraction; BS/BV = specific bone surface density; SMI = structure model index; TBPf = trabecular bone pattern factor; DA = degree of anisotropy; Tb.Th = trabecular thickness; Tb.Sp = trabecular separation; Conn.D = connectivity density; CV = coefficient of variation.

Table 2. Morphometric and Mechanical Properties of Two Specimens From the Same Donor

Sample	BV/TV (%)	Tb.Sp (mm)	Tb.Th (mm)	SMI (1)	TBPf (1/mm)	DA (1)	E (MPa)	Ultimate strength (MPa)
Fig. 2*B*	7.71	1.04	0.146	2.00	6.92	1.21	58.2	1.039
Fig. 3*C*	7.49	1.44	0.172	1.68	4.81	1.48	89.71	1.552
Difference	−3%	+38%	+18%	−16%	−30%	+22%	+54%	+49%

BV/TV = bone volume fraction; Tb.Sp = trabecular separation; Tb.Th = trabecular thickness; SMI = structure model index; TBPf = trabecular bone pattern factor; DA = degree of anisotropy; E = Young's modulus.

There were no interconnecting horizontal trabecular elements identified to provide this plate with transverse support. Figure 3*B* shows the subsection of a trabecular structure with large vertical trabeculae connected through a small number of horizontal trabeculae. The two arrows point to two horizontal trabeculae that interconnect the left part of the structure to the right part. Successive compression steps revealed that the upper trabecula was bent during compression, whereas the lower one failed in tension. In Fig. 3*C* the arrow points to a vertical plate that is optimally oriented to absorb axial loading. We found no interconnecting horizontal trabeculae to fortify this plate, which underwent catastrophic failure during the compression cycle.

In order to analyze different types of microstructures in greater detail, the two samples from Figs. 2*B* and 3*C* were selected and compared morphometrically (Table 2) because of their similar BV/TV values (7.71% versus 7.49%).

The analysis of BV/TV in the 10 subregions showed that the coefficient of variation (CV) ranged from 9.07% to 28.23%, suggesting that, although from a single donor, these samples were rather inhomogeneous. A correlation value of $R^2 = 0.57$ was obtained when correlating the lowest BV/TV of the 10 subregions to ultimate strength. This correlation was only marginally higher than that of BV/TV for the entire sample with ultimate strength ($R^2 = 0.55$; Fig. 4).

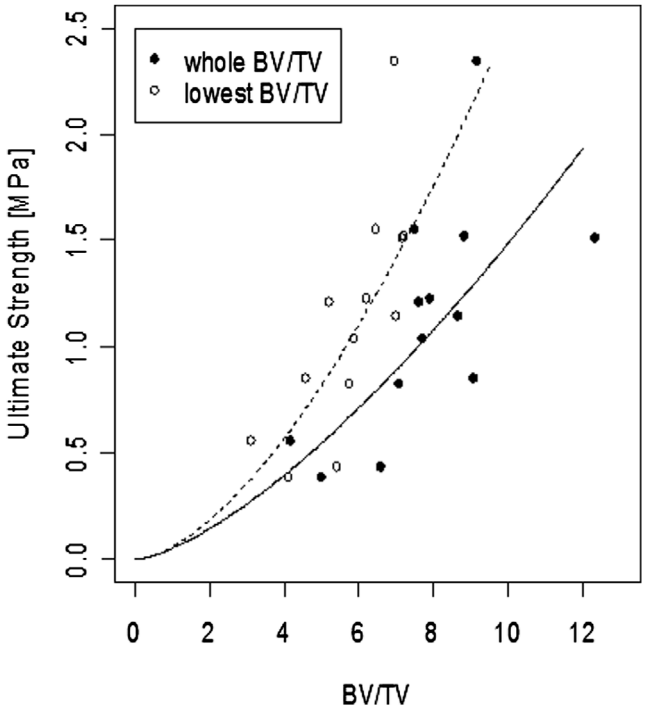

Fig. 4. Ultimate strength versus entire sample BV/TV and lowest subregion BV/TV. Limiting BV/TV to the weakest subregion did not improve the correlation. BV/TV = bone volume fraction.

Discussion

In this work, we studied the failure mechanisms of human trabecular bone samples based on IGFA.[12] Based on our visual observations, we could identify samples that failed in well-defined bands (some parts of the structure fail, whereas other remain intact), whereas others failed catastrophically over the entire sample length (no part of the structure is unaffected by failure). We suggest that failure in well-defined and localized bands primarily occurs in more homogeneous and isotropic bone samples, whereas catastrophic failure occurs in inhomogeneous and highly anisotropic bone samples. Such visual observations may help improve our understanding of failure mechanisms, which may result in new ideas to develop better morphometric indices to identify the weaknesses of trabecular bone.

We suggest that failure of homogeneous and isotropic trabecular bone is determined by the weakest configuration of all possible sets of trabeculae lying on a surface that spans across the specimen. Thus, failure in such samples occurs predominantly in well-defined bands, whereas the regions outside this band hardly undergo any deformation. This finding is supported by a study based on 2D Voronoi-derived finite element (FE) models by Silva and Gibson[44]; they reported band-like failure regions as well. The aforementioned models were extremely homogeneous and isotropic, because they were generated by mathematical algorithms. In our study, we analyzed true bone samples, in which perfect homogeneity cannot be found. Nevertheless, the samples shown in Fig. 2 all look relatively homogeneous and isotropic. In all these samples we found a well-defined region where failure occurred. This failure was found in compression mode for the sample in Fig. 2*A*, in shear mode for the sample shown in Fig. 2*C*, and in a combined compression-shear mode for the sample shown in Fig. 2*B*.

Motivated by this visual finding, we assumed that ultimate strength should be predicted more accurately by considering the BV/TV of a well-defined region of failure as opposed to the entire sample. Perilli and colleagues[45] reported that regions with minimum BV/TV values better predicted ultimate stress than average BV/TV. In this study, we correlated the lowest BV/TV value of the 10 subregions for each sample versus the ultimate strength and compared the results with the correlation of BV/TV values from the entire sample versus ultimate strength (Fig. 4). The correlation was only marginally improved, from $R^2 = 0.55$ to $R^2 = 0.57$. This finding could be explained in a number of ways. First, if all samples were extremely homogeneous, then the BV/TV in each subregion would reflect the BV/TV of the entire sample. This certainly was not the case, because we found CV values that

ranged from 9.07% to 28.23%. Thus, the variability was relatively large in all samples. Second, for specimens in which the band of failure spanned diagonally through the entire sample (Fig. 2*C*), the 10 equally divided subregions along the axis were not predictive of failure. Furthermore, images in Fig. 3 suggest that anisotropic samples tend to fail catastrophically over the entire length of the sample. Therefore, division of the sample into 10 equal subregions is unlikely to produce significant results. However, in a previous study where we took into account that failure may not be limited to one subregion only, but may occur in several subregions, we found that the lowest BV/TV is a better predictor for bone strength than the average BV/TV.[46] Nevertheless, to prove this concept, further studies are required that are able to identify the bands of failure, which could be very complex because the orientation (phi and theta) as well as the level must be identified correctly. Furthermore, the bands of failure do not necessarily have to be a plane but can take any complex-shaped surface. With this study, we aimed to provide visual input for the development of a strategy to further prove our proposed concept.

We suggest that inhomogeneous, anisotropic bone specimens tend to fail catastrophically; ie, fail over the whole region. This finding is supported by the study of Fields and colleagues,[47] who showed that diminished structural redundancy in vertebrae may be an important etiologic aspect of age-related vertebral fragility. They concluded that a reduced number of vertical load paths leads to an increase in bending-type failure of the remaining trabeculae, which further weakens trabecular bone. In this study, in Fig. 3, all samples failed over the entire length of the sample, and hardly any region remained unaffected. The sample in Fig. 3*A* failed in a barreling failure mode, where the plate-like structure on the right (arrow) was disrupted from the rest of the structure. This element was connected to the rest of the structure by a thin, horizontal trabecular element, which did not provide adequate lateral support to keep the structure from tensile failure. Had there been more horizontal trabecular elements interconnecting the vertical plate-like structures, catastrophic failure could have possibly been avoided. Similarly, the sample in Fig. 3*C* highlighted a plate-like element (arrow) that folded completely during the compression cycle. In this sample it is evident from the intact image that horizontal interconnecting trabecular elements which provide lateral support were missing. The sample in Fig. 3*B* was composed of a few strong vertical plate-like elements interconnected by only a few horizontal elements (arrows). The lower arrow points to an element that was broken in tension during failure, whereas the upper arrow points to an element that underwent bending. It is noteworthy that both of these elements were connected to the same vertical column.

The limitations of quantitative morphometry in the prediction of bone failure has been demonstrated in previous studies, in which it was shown that strength of trabecular bone specimens depends on the orientation of the applied load[10,48] and on local variations in the trabecular network.[45] Bone volume density is certainly the most important index for estimating bone strength; however, because it is a scalar, this index cannot assess orientation dependency and local weaknesses. For this reason, different approaches have been taken to include local tissue property variations and anisotropy of trabecular bone. Charlebois and colleagues[11] used a fabric tensor in addition to BV/TV; however, because they already had a good correlation with BV/TV, the fabric tensor did not add much to their correlation. Further, it has been shown that tissue mineral density may explain part of the variation in stiffness or strength, but that these contributions are small compared to mass and microstructural variations.[46] Recently, a method referred to as volumetric decomposition has been developed[49,50] to extract the rod and plate elements from the trabecular network. With this method it was shown that the mechanical properties of trabecular bone can be well predicted by including properties of single rods and plates.[50–52] Moreover, these studies revealed the specific contributions from individual trabecular rods and plates to bone strength. Although these studies showed improved predictions of bone mechanical properties, the local variations were used to derive a scalar and thus do not take into account the anisotropy of trabecular bone. This might be a reasonable approach as long as only the strength along the anatomical axis is of interest; however, for the description of trabecular bone strength along any loading direction a model describing a strength tensor should be derived from local tissue property variations. Such a tensor could be derived by FE methods, in which load is applied in a given number of directions. As voxel-based FE is computationally intensive, beam FE[53] or beam-shell FE[54] methods might be valuable alternatives.

Although all samples were harvested from the same donor, we found a large variation in bone architecture and corresponding failure modes, which is reflected in the images (Figs. 2 and 3) as well as in the morphometric indices (Table 1). The apparent BV/TV ranged from 4.19% to 12.33%, a threefold variation. Therefore, it is difficult to predict the apparent bone density at a specific site or even at other sites within the body from one trabecular bone specimen. The location where bone was taken from may be extremely sensitive; therefore, results from autopsy and biopsy studies comparing different individuals must be taken with care and cannot be extrapolated to the whole organ or even to other sites.

In this work, we have suggested two predominant failure mechanisms in trabecular bone: band failure in homogeneous specimens, and catastrophic failure in inhomogeneous specimens. However, these findings are limited to bone cores and may not be generalized to whole organs. The trabecular bone cores analyzed may fail differently within their parent organ because the boundary conditions are different. Especially, trabeculae that are cut by the coring procedure are no longer supported by the surrounding bone structure and therefore failure may be different from failure of the same structure inside the whole organ. Nevertheless, such biopsies are the gold standard in mechanical testing of trabecular bone and therefore this limitation would also affect other widely published results on material properties of trabecular bone. Because of the consistency in results from these earlier studies assessing trabecular bone mechanical properties, we believe that the mechanisms we describe here are still representative of the mechanical behavior of trabecular bone as a tissue. Additionally, because IGFA studies are very labor-intensive and time-intensive, only a limited number of bone cores could be tested and analyzed, restricting statistical power. In the future, fully validated FE approaches might help to better understand these local phenomena and with that to elucidate the heterogeneity of trabecular bone failure. Furthermore, multiple-linear regression of morphometric indices as well as including their maxima, minima, or SD may improve correlation as opposed to the use of BV/TV alone. However, such models will only capture orientation dependency if the indices included in the model are also orientation-dependent.

In conclusion, we suggest that two main failure mechanisms determine the competence of trabecular bone samples from the

same donor. Whereas in homogeneous, isotropic trabecular bone samples a whole set of trabecular elements determine the competence, in inhomogeneous and anisotropic samples a single or a missing trabeculae may be responsible for catastrophic bone failure. Because morphometric algorithms are designed to work on homogeneous trabecular bone samples, in which all trabeculae are of about the same type, these algorithms are often not capable of capturing these weaknesses and may fail in predicting bone strength under these constructions.

Disclosures

MS and RM own stock in b-cube AG and are members of the company's board of directors. AN states that he has no conflicts of interest.

Acknowledgments

This study was partly funded by a Biomedical Engineering Research Grant of the Whitaker Foundation and the SNF Professorship in Bioengineering of the Swiss National Science Foundation (FP 620-58097.99 and PP-104317/1).

Authors' roles: Study design: All authors. Data collection: MS and AN. Image processing and quantification: MS. Data interpretation: MS and RM. Statistics: MS. Writing and drafting manuscript: MS. Revising the manuscript critically for important intellectual content: AN and RM. All authors approved the final version of the manuscript. MS takes responsibility for the integrity of the data analysis.

References

1. Riggs B, Melton LJ 3rd. The worldwide problem of osteoporosis: insights afforded by epidemiology. Bone. 1995;17(5 Suppl):505S–11S.
2. Consensus development conference: diagnosis, prophylaxis, and treatment of osteoporosis. Am J Med. 1993;94(6):646–50.
3. Turner CH, Burr DB. Basic biomechanical measurements of bone: a tutorial. Bone. 1993;14(4):595–608.
4. Linde F, Hvid I, Madsen F. The effect of specimen geometry on the mechanical behaviour of trabecular bone specimens. J Biomech. 1992;25(4):359–68.
5. Keaveny TM, Borchers RE, Gibson LJ, Hayes WC. Trabecular bone modulus and strength can depend on specimen geometry. J Biomech. 1993;26(8):991–1000.
6. Keaveny TM, Guo XE, Wachtel EF, McMahon TA, Hayes WC. Trabecular bone exhibits fully linear elastic behavior and yields at low strains. J Biomech. 1994;27(9):1127–36.
7. Keaveny TM, Wachtel EF, Ford CM, Hayes WC. Differences between the tensile and compressive strengths of bovine tibial trabecular bone depend on modulus. J Biomech. 1994;27(9):1137–46.
8. Goulet R, Goldstein S, Ciarelli M, Kuhn J, Brown M, Feldkamp L. The relationship between the structural and orthogonal compressive properties of trabecular bone. J Biomech. 1994;27:375–89.
9. Odgaard A, Linde F. The underestimation of Young's modulus in compressive testing of cancellous bone specimens. J Biomech. 1991;24(8):691–8.
10. Bevill G, Farhamand F, Keaveny TM. Heterogeneity of yield strain in low-density versus high-density human trabecular bone. J Biomech. 2009;42(13):2165–70.
11. Charlebois M, Pretterklieber M, Zysset PK. The role of fabric in the large strain compressive behavior of human trabecular bone. J Biomech Eng. 2010;132(12):121006.
12. Müller R, Gerber SC, Hayes WC. Micro-compression: a novel technique for the nondestructive assessment of local bone failure. Technol Health Care. 1998;6(5–6):433–4.
13. Nazarian A, Müller R. Time-lapsed microstructural imaging of bone failure behavior. J Biomech. 2004;37(1):55–65.
14. Nazarian A, Stauber M, Müller R. Design and implementation of a novel mechanical testing system for cellular solids. J Biomed Mater Res B Appl Biomater. 2005;73(2):400–11.
15. Nazarian A, Stauber M, Zurakowski D, Snyder BD, Müeller R. The interaction of microstructure and volume fraction in predicting failure in cancellous bone. Bone. 2006;39(6):1196–202.
16. Carter DR, Hayes WC. The compressive behavior of bone as a two-phase porous structure. J Bone Joint Surg Am. 1977;59(7):954–62.
17. Rice JC, Cowin SC, Bowman JA. On the dependence of the elasticity and strength of cancellous bone on apparent density. J Biomech. 1988;21(2):155–68.
18. Keller T. Predicting the compressive mechanical behavior of bone. J Biomech. 1984;27:1159–68.
19. Judex S, Boyd S, Qin YX, Miller LR, Müller R, Rubin C. Combining high-resolution micro-computed tomography with material composition to define the quality of bone tissue. Curr Osteoporos Rep. 2003;1: 11–9.
20. Müller R, van Lenthe GH. Microarchitectural aspects of quality and competence of bone. Adv Osteoporotic Fract Manag. 2004;3:2–12.
21. Müller R, Hildebrand T, Rüegsegger P. Non-invasive bone biopsy: a new method to analyse and display the three-dimensional structure of trabecular bone. Phys Med Biol. 1994;39(1):145–64.
22. Odgaard A. Three-dimensional methods for quantification of cancellous bone architecture. Bone. 1997;20(4):315–28.
23. Hildebrand T, Rüegsegger P. A new method for the model independent assessment of thickness in three-dimensional images. J Microsc. 1997 Jan;185(1):67–75. doi: 10.1046/j.1365-2818.1997.1340694.x
24. Odgaard A, Gundersen HJ. Quantification of connectivity in cancellous bone, with special emphasis on 3-D reconstructions. Bone. 1993;14(2):173–82.
25. Hildebrand T, Rüegsegger P. Quantification of bone microarchitecture with the structure model index. Comput Methods Biomech Biomed Engin. 1997;1(1):15–23.
26. Jinnai H, Watashiba H, Kajihara T, Nishikawa Y, Takahashi M, Ito M. Surface curvatures of trabecular bone microarchitecture. Bone. 2002;30(1):191–4.
27. Hahn M, Vogel M, Pompesius-Kempa M, Delling G. Trabecular bone pattern factor-a new parameter for simple quantification of bone microarchitecture. Bone. 1992;13(4):327–30.
28. Zysset PK. A review of morphology-elasticity relationships in human trabecular bone: theories and experiments. J Biomech. 2003;36(10): 1469–85.
29. Gomberg BR, Saha PK, Wehrli FW. Topology-based orientation analysis of trabecular bone networks. Med Phys. 2003;30(2):158–68.
30. Keaveny TM, Pinilla TP, Crawford RP, Kopperdahl DL, Lou A. Systematic and random errors in compression testing of trabecular bone. J Orthop Res. 1997;15(1):101–10.
31. Nazarian A. Image-guided micro-compression: a novel technique for nondestructive assessment of bone failure [master's thesis]. Boston (MA): Boston University, College of Engineering; 2001;208 p.
32. Keaveny TM, Borchers RE, Gibson LJ, Hayes WC. Theoretical analysis of the experimental artifact in trabecular bone compressive modulus. J Biomech. 1993;26:599–607.
33. Rüegsegger P, Koller B, Müller R. A microtomographic system for the nondestructive evaluation of bone architecture. Calcif Tissue Int. 1996;58(1):24–9.
34. Balto K, Müller R, Carrington DC, Dobeck J, Stashenko P. Quantification of periapical bone destruction in mice by micro-computed tomography. J Dent Res. 2000;79(1):35–40.
35. Kapadia RD, Stroup GB, Badger AM, Koller B, Levin JM, Coatney RW, Dodds RA, Liang X, Lark MW, Gowen M. Applications of micro-CT and MR microscopy to study pre-clinical models of osteoporosis and osteoarthritis. Technol Health Care. 1998;6(5–6):361–72.
36. Müller R, Van Campenhout H, Van Damme B, Van Der Perre G, Dequeker J, Hildebrand T, Rüegsegger P. Morphometric analysis of human bone biopsies: a quantitative structural comparison of

histological sections and micro-computed tomography. Bone. 1998;23(1):59–66.

37. von Stechow D, Balto K, Stashenko P, Müller R. Three-dimensional quantitation of periradicular bone destruction by micro-computed tomography. J Endod. 2003;29(4):252–6.
38. Alexander J, Bab I, Fish S, Müller R, Uchiyama T, Gronowicz G, Nahounou N, Zhao Q, White D, Chorev M, Gazit D, Rosenblatt M. Human parathyroid hormone 1–34 reverses bone loss in ovariectomized mice. J Bone Miner Res. 2001;16:1665–73.
39. Dempster DW, Cosman F, Kurland ES, Zhou H, Nieves J, Woelfert L, Shane E, Plavetic K, Müller R, Bilezikian J, Lindsay R. Effects of daily treatment with parathyroid hormone on bone microarchitecture and turnover in patients with osteoporosis: a paired biopsy study. J Bone Miner Res. 2001;16(10):1846–53.
40. Turner CH, Hsieh YF, Müller R, Bouxsein ML, Baylink DJ, Rosen CJ, Grynpas MD, Donahue LR, Beamer WG. Genetic regulation of cortical and trabecular bone strength and microstructure in inbred strains of mice. J Bone Miner Res. 2000;15(6):1126–31.
41. Müller R, Rüegsegger P. Micro-tomographic imaging for the nondestructive evaluation of trabecular bone architecture. Stud Health Technol Inform. 1997;40:61–79.
42. Hildebrand T, Laib A, Müller R, Dequeker J, Rüegsegger P. Direct three-dimensional morphometric analysis of human cancellous bone: microstructural data from spine, femur, iliac crest, and calcaneus. J Bone Miner Res. 1999;14(7):1167–74.
43. Lorensen WE, Cline HE. Marching cubes: a high resolution 3D surface construction algorithm. Paper presented at: 14th Annual Conference on Computer Graphics and Interactive Techniques (SIGGRAPH '87); 1987 Jul 27–31; Anaheim, CA, USA [cited 2013 Jun 18]. Available from: http://doi.acm.org/10.1145/37401.37422 doi: 10.1145/37401.37422
44. Silva MJ, Gibson LJ. Modeling the mechanical behavior of vertebral trabecular bone: effects of age-related changes in microstructure. Bone. 1997;21(2):191–9.
45. Perilli E, Baleani M, Ohman C, Fognani R, Baruffaldi F, Viceconti M. Dependence of mechanical compressive strength on local variations in microarchitecture in cancellous bone of proximal human femur. J Biomech. 2008;41(2):438–46.
46. Nazarian A, von Stechow D, Zurakowski D, Müller R, Snyder BD. Bone volume fraction explains the variation in strength and stiffness of cancellous bone affected by metastatic cancer and osteoporosis. Calcif Tissue Int. 2008;83(6):368–79.
47. Fields AJ, Nawathe S, Eswaran SK, Jekir MG, Adams MF, Papadopoulos P, Keaveny TM. Vertebral fragility and structural redundancy. J Bone Miner Res. 2012;27(10):2152–8.
48. Parkinson IH, Badiei A, Stauber M, Codrington J, Müller R, Fazzalari NL. Vertebral body bone strength: the contribution of individual trabecular element morphology. Osteoporos Int. 2012; 23(7):1957–65.
49. Stauber M, Müller R. Volumetric spatial decomposition of trabecular bone into rods and plates—a new method for local bone morphometry. Bone. 2006;38(4):475–84.
50. Liu XS, Sajda P, Saha PK, Wehrli FW, Bevill G, Keaveny TM, Guo XE. Complete volumetric decomposition of individual trabecular plates and rods and its morphological correlations with anisotropic elastic moduli in human trabecular bone. J Bone Miner Res. 2008; 23(2):223–35.
51. Stauber M, Rapillard L, van Lenthe GH, Zysset P, Müller R. Importance of individual rods and plates in the assessment of bone quality and their contribution to bone stiffness. J Bone Miner Res. 2006;21(4): 586–95.
52. Liu XS, Zhang XH, Guo XE. Contributions of trabecular rods of various orientations in determining the elastic properties of human vertebral trabecular bone. Bone. 2009;45(2):158–63.
53. van Lenthe GH, Stauber M, Müller R. Specimen-specific beam models for fast and accurate prediction of human trabecular bone mechanical properties. Bone. 2006;39(6):1182–9.
54. Vanderoost J, Jaecques SV, Van der Perre G, Boonen S, D'Hooge J, Lauriks W, van Lenthe GH. Fast and accurate specimen-specific simulation of trabecular bone elastic modulus using novel beam-shell finite element models. J Biomech. 2011;44(8):1566–72.